Chemical Engineering Journal 150 (2009) 204–212

Contents lists available at ScienceDirect

Chemical Engineering Journal

journal homepage: www.elsevier.com/locate/cej

Methanol synthesis from CO_2/H_2 using Ga_2O_3–Pd/silica catalysts: Kinetic modeling

Dante L. Chiavassa, Sebastián E. Collins, Adrian L. Bonivardi, Miguel A. Baltanás*

Instituto de Desarrollo Tecnológico para la Industria Química (INTEC) (Universidad Nacional del Litoral and Consejo Nacional de Investigaciones Científicas y Técnicas), Güemes 3450, S3000GLN Santa Fe, Argentina

ARTICLE INFO

Article history:
Received 19 November 2008
Received in revised form 10 February 2009
Accepted 11 February 2009

Keywords:
CO_2 recycling
Methanol synthesis
Palladium
Gallium oxide
Kinetic modeling

ABSTRACT

The synthesis of methanol from CO_2/H_2 on a Ga_2O_3–Pd/silica catalyst, together with the reverse water gas shift reaction, was modeled for a wide range of temperatures (508–538 K), pressures (1–4 MPa), compositions (H_2/CO_2 = 1, 3 and 6) and space velocity conditions. The kinetic information was combined with relevant spectroscopic (FT-IR) data. The rate determining steps (*rds*) of the reactions were the hydrogenation of the formate intermediate, and its decomposition on the gallia surface, respectively.

A competitive adsorption mechanism, where adsorbed atomic hydrogen occupies the same active sites as other oxygenated surface intermediates on the gallia, was found as the most satisfactory, in terms of physicochemical significance of the parameter estimates. Minimal residuals were found when considering as kinetically relevant the simultaneous surface occupancy by formate, methylenebisoxy, hydroxyl and atomic hydrogen intermediates.

The deleterious impact of CO for certain process conditions, such as high conversion and/or ternary $H_2/CO_2/CO$ mixture feeds, was also studied. In these cases, CO competes with H_2 on the Pd crystallites, severely limiting the availability of atomic hydrogen to the gallia surface. Using the steady-state approximation, the supply and demand of atomic hydrogen were then balanced to find the best model interpretation of the observed reactivity.

1. Introduction

The kinetic modeling of methanol synthesis from syngas, CO_2/H_2 and $CO/CO_2/H_2$ mixtures using industrial (i.e., $Cu/ZnO/Al_2O_3$) catalysts has been widely studied and – in general – there is nowadays ample agreement with regard to mechanistic aspects and the relevant reaction intermediates on these materials [1–3]. For CO as carbon source, for instance, it is generally accepted that the rate determining step (*rds*) is the hydrogenation of surface methoxy [4,5], whereas the reaction pathway from CO_2 to methanol follows the 'formate route' where the *rds* is the hydrogenation of formate [6]. In the kinetic modeling of the synthesis reaction using these catalysts, the participation of different types of catalytic sites has also been put forward, where the dissociation of H_2 takes place onto one of these types and the chemisorption/reaction of carbon dioxide proceeds onto another [7,8].

A similar situation arises regarding the hydrogenation of CO_2/H_2 mixtures on Ga_2O_3–Pd/silica catalysts. The supported palladium crystallites, due the high H_2 dissociation capability of the metal, generate active H_s species which then migrate to surface Ga_2O_3 patches, thereby hydrogenating the chemisorbed CO_2; a bifunctional mechanism seems to be fully operational here [9,10].

Each of the reaction intermediates involved in the synthesis of methanol from CO_2/H_2 or CO/H_2 mixtures on Ga_2O_3–Pd/silica catalysts were identified in previous work by our group using, mostly, FT-IR [10,11]. The influence of other reaction products (carbon monoxide, water, and DME) was also analyzed, via an experimental program carried out under typical process conditions. The experiments were conducted using a plug-flow, differential reactor and a Berty-type CSTR recycle reactor, for a wide range of temperature (508–538 K), pressure (1–4 MPa), composition (H_2/CO_2 = 1, 3 and 6), and space velocity, including H_2–CO–CO_2 and H_2–He–CO_2 ternary mixtures as well [12].

Nevertheless, it was deemed convenient to analyze the reacting system in more detail, in order to determine whether the same *rds* is responsible for the observable macrokinetics while operating under such wide range of process variables, and to identify which chemisorbed intermediates participate in the synthesis pathway. Therefore, in this work, a detailed reaction scheme for the conversion of CO_2/H_2 and $CO_2/CO/H_2$ mixtures over a Ga_2O_3–Pd/silica catalyst is proposed, serving as the basis for the development of a mechanistically sound kinetic model. This reaction scheme accounts for the hydrogenation to methanol and includes the reverse water gas shift. Catalytic activity data obtained in the above-

* Corresponding author. Tel.: +54 342 455 9175; fax: +54 342 455 0944.
E-mail address: tderliq@santafe-conicet.gov.ar (M.A. Baltanás).

1385-8947/$ – see front matter © 2009 Elsevier B.V. All rights reserved.
doi:10.1016/j.cej.2009.02.013

mentioned experimental program [12] and complementary FT-IR information will be used in a synergistic fashion.

2. Experimental

2.1. Catalyst preparation

A stock material, with 2 wt.% Pd loading, was obtained by ion exchanging palladium acetate at pH 11 in NH_4OH(aq) onto a mesoporous silica support (Davison G59). The support was previously crushed and sieved through an 80-mesh Tyler screen, purified, calcined at 773 K and characterized (specific surface = 301 $m^2\,g^{-1}$; avg. pore diameter = 160 Å; avg. particle diameter = 52 μm). Then, $Ga(NO_3)_3$(aq), was added by incipient wetness impregnation, so as to obtain a Ga/Pd = 3 atomic ratio. Water was eliminated by sublimation at reduced pressure. The material was then calcined in air (200 $cm^3\,min^{-1}$) at 623 K (2 h), reduced under 5% H_2 in argon (200 $cm^3\,min^{-1}$) at 723 K (2 h) and passivated with oxygen pulses, prior to use.

The catalyst was stabilized by flowing consecutively mixtures of H_2/CO_2 = 3 (20 h) and then H_2/CO = 3 (12 h), followed by pure H_2 (10 h), under typical methanol synthesis process conditions: 523 K, 3 MPa. The material was then cooled to room temperature (RT) under hydrogen flow and air-passivated again. This sequence ensured a constant exposed metal fraction (from now on designated as FE), equal to 4%, throughout the experimental program [12]. The specific surface of the stabilized, powdered catalyst was 278 $m^2\,g^{-1}$. For comparison purposes (see below), an aliquot of the ion-exchanged Pd (2 wt.%)/silica base stock was subjected to the same sequence of preparation and stabilization steps. The exposed metal fraction of this stabilized material was FE = 13%.

2.2. Catalyst evaluation

The catalyst performance was evaluated using an insulated, pressurizable internal recycle Berty-type CSTR reactor (500 cm^3), furnished with its own PID temperature controller (Autoclave Engineers Inc.), to collect data at integral conversion values in the absence of extraparticle mass- or heat-transfer resistances. The absence of internal diffusional limitations was thoroughly verified using well-established methods [13] and, so, a pseudohomogeneous model was applied [14].

The inner parts of the reactor were gold plated, *via* electrolytic deposition, to ensure total inertness of the device. The system pressure was maintained with a membrane back pressure controller. In the feed section of the setup, the reactant gas flows were controlled using Brooks 5850 TR mass-flow units. The exit lines from the reactor were inert (glass-lined stainless steel), and were constantly kept above 393 K to prevent any condensation of the reaction products, using electrical resistance heat wiring.

The stock of stabilized, air-passivated (powdered) catalyst was pelletized using a 13 mm dia. hardened stainless steel die and a hydraulic press, employing enough amount of powdered catalyst each time so as to get about 1-mm thick pellets (applied pressure ≈ 380 MPa/cm^2 during ≈10 min) and then gently crushed the pellets into small particles of about 1 mm diameter (Specific surface of the pelletized catalyst = 233 $m^2\,g^{-1}$). Prior to each run a fresh load of the catalyst was reduced in situ under H_2, with a heating rate of 3 K/min from RT to 523 K, then maintaining the last temperature for 1 h. A wide range of temperatures (508–538 K), pressures (1–4 MPa), compositions (H_2/CO_2 = 1, 3 and 6), and space velocities ($W/F^0_{CO_2}$) was used, including H_2/CO_2/CO ternary mixtures as well. To discriminate mechanistic differences, further runs were done using the base stock material Pd (2 wt.%)/silica, under similar process conditions.

The exit gas composition was analyzed by GLC in two Shimadzu 9A units arranged in parallel, employing Porapak QS and Carbosieve SII filled (1/8 in. ID, 3 m long) stainless steel columns.

A total of 347 integral experimental data were taken with the Ga_2O_3–Pd/silica catalyst and another set of 144 data points were taken (P = 3 MPa) using the Pd (2 wt.%)/silica [15]. For illustration purposes some of these data – taken at 538 K – are shown in Table 1. Exit composition and percent carbon conversion values are included in the table, to show that even for the maximum CO_2 conversion data ($X_{CO_2} \sim 7\%$) the CSTR was operating far from thermodynamic equilibrium.

3. Reaction mechanism and derivation of the kinetic equations

Based on former studies, we can safely assume that CO_2 is the main source of carbon in the methanol synthesis on the Ga_2O_3–Pd/silica catalyst from H_2/CO_2/CO mixtures [10,16–18]:

$$CO_2 + 3H_2 \leftrightarrows CH_3OH + H_2O \quad (R1)$$

Nonetheless, a proper description of the reaction system must also account for the water gas shift or, more correctly, its reverse (RWGS) reaction:

$$CO_2 + H_2 \leftrightarrows CO + H_2O \quad (R2)$$

Both reactions proceed on the gallia phase of the catalyst. Yet, since the pioneering work of Poutsma and co-workers [19], Pd/silica catalysts are known to produce methanol from syn-gas on the metal crystallites, with good selectivity, via:

$$CO + 2H_2 \leftrightarrows CH_3OH \quad (R3)$$

From a thermodynamic point of view, only two of these reactions are independent and – whenever the formation of DME is just minor, as is the case with these Ga_2O_3–Pd/silica catalysts [16] – they suffice to fully describe the reaction system. Using a CSTR, the reaction rates can be directly found from the mass balances of each species. Under steady-state conditions, two time-independent responses completely describe the system, so that only two continuity equations (e.g., for CH_3OH and CO) have to be considered.

Silica-supported palladium is also capable of producing CH_3OH and CO from CO_2/H_2 mixtures [20], and this was confirmed in the additional runs that were carried out using the stabilized Pd (2 wt.%)/silica base stock [12,15]. For each experimental condition, the specific reaction rate to methanol (through reactions R1 and R3) was *vis-à-vis* much smaller – about two orders of magnitude less – on Pd/silica than on the Ga_2O_3–Pd/silica catalyst (see, for example, Fig. 5 in Ref. [12]). In a like manner, although the *specific* reaction rate to CO is by no means negligible on Pd/silica, it can be safely disregarded as well – as compared to the Ga_2O_3–Pd/silica catalyst – because it represents at most up to 4% of what the latter produced under identical process conditions [12,15].

3.1. Competitive and uncompetitive hydrogen adsorption models

Recent work by Collins et al. [9,10] has shown that the synthesis of methanol from H_2/CO_2 on these Ga_2O_3–Pd catalysts follows a stepwise carbonate–formate–methylenebisoxi–methanol hydrogenation pathway, on the on the reduced gallium oxide surface, which is similar to the hydrogenation route found by Bell and co-workers for Cu/SiO_2 and $Cu/ZrO_2/SiO_2$ [21–23] (Fig. 1). Labile gallium carbonates are formed in the first, CO_2 chemisorption step, using exposed (i.e., 'bare') oxygen atoms of the gallium oxide. This oxygen species will be indicated as O-* from now on, to denote that the oxygen atom is bound to a surface gallium (a * represents an available surface gallium site). Each of the reduction

Table 1
Comparative reaction rates, CO_2 conversion and approach to thermodynamic equilibrium, for different values of the reactants ratio, total pressure and space velocity, using the Ga_2O_3–Pd/SiO_2 catalyst in the Berty-type CSTR reactor (T = 538 K).

H_2/CO_2	P_{TOTAL} (MPa)	$W/F^0_{CO_2}$ ($\times 10^{-3}$ g_{cat} s/mol)	R_{MeOH} ($\times 10^8$ mol/g_{cat} s)	y_{H_2O} (%)[a]	y_{CO} (%)[a]	X_C (%)		$(X_C^{EXP}/X_C^{EQ}) \times 100$
						EXP	EQ	
		2.62	390.1	0.42	0.16	1.64		7.22
		4.73	297.1	0.61	0.24	2.32		10.2
3	3	9.28	211.5	0.91	0.37	3.38	22.72	14.8
		18.9	140.7	1.23	0.54	4.79		21.1
		46.7	83.2	1.79	0.82	7.46		32.8
		2.77	425.9	0.48	0.18	1.86		7.69
		5.07	335.3	0.67	0.26	2.71		11.22
3	4	10.1	248.3	1.04	0.42	4.16	24.16	17.22
		17.6	192.9	1.57	0.68	5.98		24.75
		39.2	107.9	1.90	0.96	7.77		32.16
		2.49	257.8	0.28	0.12	1.07		5.29
		4.60	227.1	0.49	0.21	1.84		9.09
3	2	8.73	157.8	0.66	0.29	2.45	20.24	12.10
		17.9	108.3	0.95	0.43	3.59		17.74
		40.8	67.3	1.44	0.71	5.57		27.52
		2.45	149.5	0.17	0.08	0.66		3.47
		4.49	133.6	0.29	0.14	1.12		5.89
3	1	9.11	106.8	0.48	0.23	1.89	19.00	9.95
		17.2	76.3	0.72	0.37	2.76		14.53
		40.2	44.1	1.06	0.57	4.08		21.47
		2.65	352.2	0.21	0.08	1.38		4.38
		4.98	310.5	0.34	0.12	2.34		7.43
6	3	10.5	232.9	0.53	0.19	3.79	31.51	12.03
		18.3	184.3	0.78	0.31	5.38		17.07
		39.7	114.4	1.03	0.43	7.39		23.45
3	3	2.62	325.6	0.37	0.13	1.34	22.72	5.90
		2.55	235.3	0.65	0.30	1.16		9.80
		4.45	164.2	0.81	0.39	1.45		12.25
1	3	8.96	108.7	1.19	0.61	2.09	11.84	17.65
		17.7	66.1	1.66	0.91	2.81		23.73
		34.9	41.9	2.07	1.37	3.97		33.53
3	3	3.46	325.6	0.37	0.13	1.34	22.72	5.90
		3.63	294.0	0.30	0.20 (0.06)	1.30	21.92	5.93
		6.48	240.1	0.46	0.33 (0.15)	1.86	21.68	8.58
[b]	3	13.3	172.4	0.66	0.58 (0.32)	2.61	21.32	12.24
		24.9	125.9	0.95	1.02 (0.64)	3.81	20.68	18.42
		52.9	73.1	1.36	1.86 (1.28)	5.85	19.36	30.22
3	3	50.9	71.9	1.57	0.69	7.22	22.72	31.78

[a] Percent mole fraction at the reactor exit.
[b] Mixture $H_2/(CO_2 + CO) = 3$. The y_{CO} values between parentheses correspond to mol% CO in the feed.

steps consumes atomic hydrogen, which is supplied from the palladium crystallites, onto which H-• species are formed via the fast chemisorption/dissociation of H_2(g) (• represents available, surface Pd sites). The H-• species then migrate to the metal–gallia interface and diffuse onto the GaO_x phase as mobile H-* species, which are the actual reducing species. This point of view can be labeled the 'competitive' hydrogen adsorption model model, because CO_2, hydrogen and the oxygenated intermediates can occupy the same * sites of the gallia surface. In practical terms, this implies that the H-* species behave as surface hydrides and, indeed, this species can be detected by FT-IR on Ga_2O_3–Pd/silica above 473 K [24]. An alternate point of view, the 'non-competitive' hydrogen adsorption model, will be presented in the following paragraphs.

Regarding the formation of CO on the gallia surface, one must bear in mind that CO_2 does *not* dissociate onto Ga_2O_3 to give O-* and CO(ads) species [25]. A plausible decomposition of some of the carbonaceous intermediates has to be considered, instead, using the following piece of experimental information: Infrared spectra of CO chemisorbed on gallia in the absence of hydrogen have shown that the exposure to carbon monoxide leads to surface dehydroxylation, and, thence, to formate formation [26,27]. Thus, it is entirely congruent to pose that the RWGS reaction proceeds on GaO_x following an inverse path, whereby formate decomposition involves the following reaction step:

$$HCO_2\text{-}* \leftrightarrows HO\text{-}* + CO(g)$$

The complete set of elementary steps that lead to both methanol and carbon monoxide is shown in Table 2; all of them are reversible.

Using the LHHW formalism, the *rds* for carbon monoxide formation is step 12 (S12), since it is the only one that produces CO (see later). For methanol, S1 and S2 can be entirely ruled out as rate determining steps, as gallium carbonates are known to be highly reactive under reaction conditions [10,18]. In addition, steps S6 and S9 can be disregarded as *rds* because the adsorption/desorption equilibria of CH_3OH and H_2O on gallia are fast [28]. Likewise, steps S7 and S8, which involve the re-hydroxylation of the surface via the highly reactive H-* species, are fast on most oxides [29]. Finally, step S4 must be dismissed as well as *rds* because methylenebisoxy intermediaries are extremely reactive. They have never been observed under steady-state reaction conditions but, rather, in transient experiments or under reactants-depleted con-

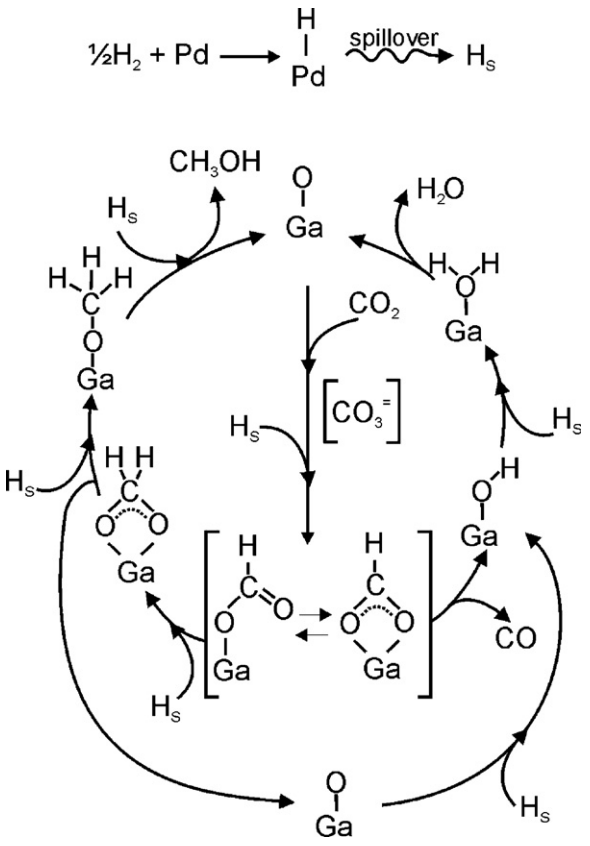

Fig. 1. Methanol synthesis and reverse water gas shift reaction (RWGS) on the Ga_2O_3–Pd/silica catalyst: reaction scheme.

ditions on Ga_2O_3–Pd/silica and Ga_2O_3/silica [10,11,28], or Cu/silica [21–23] surfaces.

The most likely rate controlling steps left are, therefore, the hydrogenations of either formate (S3) or methoxide (S5). The derivation of the corresponding sets of kinetic equations using each of these steps as *rds* was performed. However, the parameter estimation procedure (*vide infra*) yielded negative values when S5 was considered as the *rds* and, so, from now on we will only discuss the derivation of the model equations using S3 to account for the methanol formation rate:

$$r_3 = k_3[HCO_2\text{-}*][H\text{-}*] - k_{-3}[H_2CO_2\text{-}*][*] \quad (1)$$

Table 2
Competitive adsorption model: outline of the reaction pathway.

Elementary reaction step	Step code	Intermediate, molecule, or process
Onto gallia		
$CO_2(g) + O\text{-}* \leftrightarrows CO_3\text{-}*$	(S1)	Carbonate
$CO_3\text{-}* + H\text{-}* \leftrightarrows HCO_2\text{-}* + O\text{-}*$	(S2)	Formate
$HCO_2\text{-}* + H\text{-}* \leftrightarrows H_2CO_2\text{-}* + *$	(S3)	Methylenebisoxy
$H_2CO_2\text{-}* + H\text{-}* \leftrightarrows H_3CO\text{-}* + O\text{-}*$	(S4)	Methoxi
$H_3CO\text{-}* + H\text{-}* \leftrightarrows H_3COH\text{-}* + *$	(S5)	Methanol
$H_3COH\text{-}* \leftrightarrows H_3COH(g) + *$	(S6)	Desorption
$O\text{-}* + H\text{-}* \leftrightarrows HO\text{-}* + *$	(S7)	Hydroxyl
$HO\text{-}* + H\text{-}* \leftrightarrows H_2O\text{-}* + *$	(S8)	Water
$H_2O\text{-}* \leftrightarrows H_2O(g) + *$	(S9)	Desorption
Onto Pd		
$H_2 + 2\bullet \leftrightarrows 2\,H\text{-}\bullet$	(S10)	Dissociation
Onto Pd/gallia		
$H\text{-}\bullet + * \leftrightarrows H\text{-}* + \bullet$	(S11)	Migration
Onto gallia		
$HCO_2\text{-}* \leftrightarrows HO\text{-}* + CO(g)$	(S12)	Decomposition

For CO formation, on the other hand, the S12 (an Eley-Rideal CO adsorption) step gives the following expression:

$$r_{12} = k_{12}[HCO_2\text{-}*] - k_{-12}p_{CO}[HO\text{-}*] \quad (2)$$

Within the LHHW formalism, the remaining reaction steps (S1, S2, and S4–S11) are in equilibrium and can be used to calculate the surface concentration of each reaction intermediate. Table 3 contains the complete set of these concentrations (indicated by g_j in the table). Next, using the total balance of surface sites on the gallia, $[*]_T$:

$$r_3 = \frac{k'_3 p_{CO_2} p_{H_2}(1 - (p_{CH_3OH}p_{H_2O}/p^3_{H_2}p_{CO_2}K_{R1}))}{D^2} \quad (3)$$

$$r_{12} = \frac{k'_{12} p_{CO_2}\sqrt{p_{H_2}}(1 - (p_{CH_3OH}p_{H_2O}/p_{H_2}p_{CO_2}K_{R2}))}{D} \quad (4)$$

in which

$$k'_3 = k_3K_1K_2K_{10}K^2_{11}[*]^2_T; \quad k'_{12} = k_{12}K_1K_2\sqrt{K_{10}}K_{11}[*]_T \quad (5)$$

and

$$D = \frac{[*]_{tot}}{[*]} = 1 + \sum_{j=1}^{9} g_j \quad (6)$$

The respective equilibrium constants, K_{R1} and K_{R2}, are thermodynamically determined. Their values were calculated using well-established databases [30].

Table 3
Competitive adsorption model: equilibrium concentration of adsorbed intermediates or molecules.

Intermediate or molecule	Equilibrium concentration group	Group code[a]
Carbonate	$[CO_3\text{-}*] = K_1K_2p_{CO_2}p_{H_2O}/K_7K_8K_9K_{10}K^2_{11}\sqrt{p_{H_2}}[*]$	g_1
Formate	$[HCO_2\text{-}*] = K_1K_2\sqrt{K_{10}}K_{11}p_{CO_2}\sqrt{p_{H_2}}[*]$	g_2
Methylenebisoxy	$[H_2CO_2\text{-}*] = p_{CH_3OH}p_{H_2O}[*]/K_4K_5K_6K_7K_8K_9K^2_{10}K^4_{11}p^2_{H_2}$	g_3
Methoxide	$[H_3CO\text{-}*] = p_{CH_3OH}[*]/K_5K_6\sqrt{K_{10}}K_{11}\sqrt{p_{H_2}}$	g_4
Methanol	$[H_3COH\text{-}*] = p_{CH_3OH}[*]/K_6$	g_5
Oxygen	$[O\text{-}*] = p_{H_2O}[*]/K_7K_8K_9K_{10}K^2_{11}p_{H_2}$	g_6
Hydroxyl	$[HO\text{-}*] = p_{H_2O}[*]/K_8K_9\sqrt{K_{10}}K_{11}\sqrt{p_{H_2}}$	g_7
Water	$[H_2O\text{-}*] = p_{H_2O}[*]/K_9$	g_8
Hydrogen	$[H\text{-}*] = \sqrt{K_{10}}K_{11}\sqrt{p_{H_2}}[*]$	g_9

[a] These group codes correspond to each term in Eq. (6) in the text.

Table 4
Non-competitive adsorption model: outline of the reaction pathway.

Elementary reaction step	Step code	Intermediate, molecule, or process
Onto gallia		
$CO_2(g) + O\text{-}^* \leftrightarrows CO_3\text{-}^*$	(S1)	Carbonate
$CO_3\text{-}^* + H\text{-}\circ + {}^* \leftrightarrows HCO_2\text{-}^* + O\text{-}^* + \circ$	(S2)	Formate
$HCO_2\text{-}^* + H\text{-}\circ \leftrightarrows H_2CO_2\text{-}^* + \circ$	(S3)	Methylenebisoxi
$H_2CO_2\text{-}^* + H\text{-}\circ + {}^* \leftrightarrows H_3CO\text{-}^* + O\text{-}^* + \circ$	(S4)	Methoxi
$H_3CO\text{-}^* + H\text{-}\circ \leftrightarrows H_3COH\text{-}^* + \circ$	(S5)	Methanol
$H_3COH\text{-}^* \leftrightarrows H_3COH(g) + {}^*$	(S6)	Desorption
$O\text{-}^* + H\text{-}\circ \leftrightarrows HO\text{-}^* + \circ$	(S7)	Hydroxyl
$HO\text{-}^* + H\text{-}\circ \leftrightarrows H_2O\text{-}^* + \circ$	(S8)	Water
$H_2O\text{-}^* \leftrightarrows H_2O(g) + {}^*$	(S9)	Desorption
Onto Pd		
$H_2 + 2\bullet \leftrightarrows 2\,H\text{-}\bullet$	(S10)	Dissociation
On Pd/gallia		
$H\text{-}\bullet + \circ \leftrightarrows H\text{-}\circ + \bullet$	(S11′)	Migration
On gallia		
$HCO_2\text{-}^* \leftrightarrows HO\text{-}^* + CO(g)$	(S12)	Decomposition

So, the calculated (i.e., model-estimated values) of the reaction rates can be rewritten as follows:

$$< r_{CH_3OH} >_{cal} = r_3; \quad < r_{CO} >_{cal} = r_{12} \tag{7}$$

Some authors have postulated that the reactive hydrogen species chemisorbs in some metal oxides on surface sites other that those occupied by the carbonaceous species [5–7,31], which would imply that hydrogen and carbon-containing species chemisorptions are non-competitive. In mechanistic terms, considering our FT-IR spectroscopic data for the gallium oxide surface [9–11,24–26,28], this alternative can be readily formalized using a similar catalytic sequence given in Table 4, where the key reaction step is now the following:

$$H\text{-}\bullet + \circ \leftrightarrows H\text{-}\circ + \bullet \quad (S11') \quad \text{Migration ('spillover')}$$

Using a reasoning similar to that of the competitive model and considering again steps S3 and S12 as *rds*, the new alternate rate expressions for r_3 and r_{12} are now:

$$r_3 = k_3\,[HCO_2\text{-}*]\,[H\text{-}\circ] - k_{-3}\,[H_2CO_2\text{-}*][\circ] \tag{8}$$

$$r_{12} = k_{12}[HCO_2\text{-}*] - k_{-12}p_{CO}[HO\text{-}*] \tag{9}$$

A balance of total [∘] sites on the gallia: $[\circ]_T = [H\text{-}\circ] + [\circ]$, led to expressions similar to Eqs. (3) and (4), namely:

$$r_3 = \frac{k'_3 p_{CO_2} p_{H_2}(1 - (p_{CH_3OH}p_{H_2O}/p^3_{H_2}p_{CO_2}K_{R1}))}{DD_H} \tag{10}$$

$$r_{12} = \frac{k'_{12} p_{CO_2}\sqrt{p_{H_2}}(1 - (p_{CH_3OH}p_{H_2O}/p_{H_2}p_{CO_2}K_{R2}))}{D} \tag{11}$$

in which

$$k'_3 = k_3K_1K_2K_{10}K^2_{11}[*]_T[\circ]_T; \quad k'_{12} = k_{12}K_1K_2\sqrt{K_{10}}K_{11}[*]_T \tag{12}$$

$$D = 1 + \sum_{j=1}^{8} g_j \tag{13}$$

and

$$D_H = 1 + \sqrt{K_{10}}K_{11}\sqrt{p_{H_2}}[\circ] \tag{14}$$

The g_j groups indicated in Eq. (13) are identical to those defined in Table 3. It is apparent that this model accounts for an independent surface occupancy with atomic hydrogen, via the second denominator in Eq. (10), D_H. However, none of the multiresponse, non-linear regressions that were tried using this model, following the procedure outlined below, gave acceptable residuals with physically meaningful – that is, positive – values of the calculated activation energies, and so no further consideration will be given to the non-competitive model henceforth.

The parameter estimation was performed as outlined by Bard [32]. Parameter estimates were obtained by minimizing the logarithm of the determinant of the variance–covariance matrix of the response(s) residues [33], M, as the objective function, the elements of which are the following:

$$\begin{aligned} M_{11} &= \sum((r_{CH_3OH})_{exp} - < r_{CH_3OH} >_{cal})^2 \\ M_{12} = M_{21} &= \sum((r_{CH_3OH})_{exp} - < r_{CH_3OH} >_{cal})((r_{CO})_{exp} - < r_{CO} >_{cal}) \\ M_{22} &= \sum((r_{CO})_{exp} - < r_{CO} >_{cal})^2 \end{aligned} \tag{15}$$

By applying this non-linear least squares (NLLS) algorithm, a further quadratic expansion of the objective function allows estimating the confidence level of each model parameter (given the inherent experimental errors of chromatographic data, a 95% confidence level is usually chosen). Each of the model constants (*viz.*, kinetic rate and/or thermodynamic equilibria) can be written in Arrhenius or Van't Hoff forms as: $A(i)\exp(B(i)/T)$, where $B(i)$ represents either an activation energy, $\Delta E/R$, an enthalpy of reaction $-\Delta H/R$, or a combination of those. To reduce computational difficulties arising from the strong correlation between frequency factors and activation energies, these model constants were reparametrized as

$$A^*(i)\,\exp\left\{B(i)\left[\frac{1}{T_{av}} - \frac{1}{T}\right]\right\} \tag{16}$$

in which T_{av} equals 523.16 K.

To initialize the optimization routine, 'experimental values' of the apparent activation energies of r_{CH_3OH} and r_{CO} were used. Said values were calculated using the multiresponse routine and the simple power-law kinetic rate model:

$$r(i) = k(i)\Pi p_m^{\nu_{mi}} \tag{17}$$

where ν_{mi} stands for the reaction order of the mth component in the ith reaction (in our case, r_{CH_3OH} and r_{CO}) and each $k(i)$ was used in the format given by Eq. (16). These apparent activation energies were $\Delta E_{CH_3OH} = 81.0$ kJ/mol and $\Delta E_{CO} = 83.9$ kJ/mol, respectively.

Both kinetic rate constants include the product $\sqrt{K_{10}}K_{11}$, which is also present in many of the g_j groups and, as an independent parameter, in the g_9 (hydrogen chemisorption) term of D. This parameter-coupling drawback could be satisfactorily overcome by setting the initial values of ΔE_{CH_3OH} and ΔE_{CO} to fixed magnitudes during the first iterations and 'releasing' them later to obtain the final (convergence) estimates.

Fourier-transform infrared spectroscopy is an extremely powerful technique for studying catalytic processes *in situ*. Not just plausible but actually observable reaction intermediates have thus been positively identified. Despite this significant progress, scant work is yet available under true *operando* conditions (i.e., under real pressure, temperature, and space velocities). Even then, the specific absorbance (or absorptivity) of chemisorbed species is usually not known. Hence, the complete set of reaction intermediates that give infrared signals in the 508–538 K range on the Ga_2O_3–Pd/silica catalyst [9–11] was kept as possible adsorbed candidates to be retained in the D expression. So, after several trials trials in which at least three different adsorbates were assumed, the near-best regression (i.e., the one that gave minimal residuals *and* physically significant parameters) was obtained retaining the g_2, g_3, and g_9 terms of Table 3 or, in other words, considering the joint occupancy by formate, methylenebisoxy, and dissociated hydrogen onto the gallia (this is denoted the "239" model in Table 5). Yet, the model's abil-

Table 5
Competitive adsorption model: weighted residuals obtained for each response, considering the most relevant (adsorbed) reaction intermediates.[a].

	Adsorbates included in the D term of Eqs. (3) and (4)—see Table 3			
	239	2379	239(a)[b]	2379(a)[b]
Weighted residual[c]				
Res 1	7.98×10^{-2}	2.99×10^{-2}	7.72×10^{-2}	2.07×10^{-2}
Res 2	5.34×10^{-2}	5.83×10^{-2}	3.15×10^{-2}	4.06×10^{-2}
det M	8.34×10^{3}	8.24×10^{3}	7.33×10^{3}	7.17×10^{3}
Npar	10	12	10	12
Nobs	347	347	315	315

[a] The designation 239 stands for the model variant in which the joint occupancy by formate, methylenebisoxy and dissociated hydrogen onto the gallia (g_2, g_3, and g_9 terms of Table 3) was retained. The designation 2379 stands for the model variant in which the hydroxyl adsorbate is also considered.

[b] The last two columns correspond to the calculations made by excluding the experimental data in which CO was deliberately added to the reacting mixture.

[c] Each relative percent error of the regression residuals was weighted dividing by the total number of experimental observations (Nobs):

$$\text{Res 1} = \left\{ \sum_{i=1}^{\text{Nobs}} \left[\frac{< r_{CH_3OH} >_{exp} - < r_{CH_3OH} >_{cal}}{< r_{CH_3OH} >_{exp}} \right]^2 / \text{Nobs} \right\} \times 100$$

$$\text{Res 2} = \left\{ \sum_{i=1}^{\text{Nobs}} \left[\frac{< r_{CO} >_{exp} - < r_{CO} >_{cal}}{< r_{CO} >_{exp}} \right]^2 / \text{Nobs} \right\} \times 100$$

ity to include the impact of water was judged crucial, because an excess of surface hydration was found to be detrimental to the catalyst's performance during our experimental program [12]. Indeed, an additional inclusion of the hydroxyl groups (g_7 term in D) gave the best results. For simplicity, we will designate this model variant as the 2379 version of the competitive adsorption model. Noteworthily, whenever the methylenebisoxy term (g_3) was excluded from the runs none of the alternate model variants gave physicochemically meaningful parameters or satisfactory residuals.

Table 5 shows the NLLS residuals for both responses, weighted by dividing by the total number of experimental points in each case. These residuals further decreased upon excluding the subset of experimental runs (a total of 32 data points) where no CO had been deliberately added to the reacting mixture [residuals for this case indicated with an (a) in Table 5]; however, for all cases shown in Table 5 all rate parameters were statistically significant. As an example, Table 6 gives the model predictions for the 2379(a) case. At the 95% confidence level all the pre-exponential factors are positive. The corresponding $t_{0.95}$ values, which are approximate since the model is not linear in the parameters, were always above 2.

Parity plots, showing the excellent agreement between model predictions and experimental data for r_{CH_3OH} and r_{CO} at all conversions in the complete range of temperatures, pressures and H_2/CO_2 ratios, are displayed in Fig. 2. However, an important bias was found whenever carbon monoxide was deliberately added to the reaction mixture (as indicated by the open triangles in Fig. 2). In those cases, both the 2379 and 2379(a) variants of the model predicted higher reactivity than was experimentally observed. Fortunately, an improved microkinetic model introducing the steady-state concept (which is developed in the following section) allowed us to overcome the hurdle.

Lastly, it is worth mentioning that the use of fugacities, rather than partial pressures, was also considered, applying the Soave–Redlich–Kwong equation of state [30,34,35]. The compressibility factors were never outside the 0.99–1.10 range and so using fugacities was found to give negligible changes in the results.

Table 6
Parameter values for the competitive adsorption model, variant 2379(a).

Group source	Group component[a]	Value	Lower limit (95% conf. int.)	Upper limit (95% conf. int.)
k_3	A	$1.44 \times 10^{+4}$	$1.16 \times 10^{+4}$	$1.72 \times 10^{+4}$
	ΔE	31.01	5.18	56.78
k_{12}	A	$3.80 \times 10^{+7}$	$3.41 \times 10^{+7}$	$4.19 \times 10^{+7}$
	ΔE	65.60	52.06	79.06
g_2	A	1.18×10^{-7}	1.01×10^{-7}	1.34×10^{-7}
	$(-\Delta H)$	53.04	31.76	74.32
g_3	A	$7.54 \times 10^{+2}$	$2.76 \times 10^{+2}$	$1.22 \times 10^{+3}$
	$(-\Delta H)$	17.54	−52.13	87.30
g_7	A	8.28×10^{-5}	7.04×10^{-5}	9.52×10^{-5}
	$(-\Delta H)$	56.45	30.85	82.06
g_9	A	$2.82 \times 10^{+10}$	$8.46 \times 10^{+9}$	$4.78 \times 10^{+10}$
	$(-\Delta H)$	−118.9	−182.1	−54.46

[a] The values of the frequency factors shown in the table correspond to either Arrhenius or Van't Hoff propositions—see text. ΔE and ΔH values are given in kJ/mol.

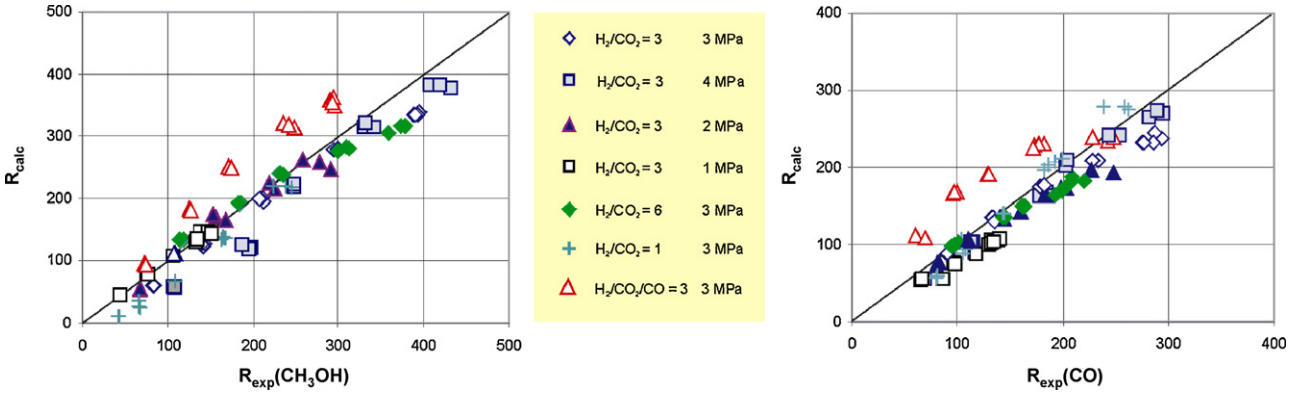

Fig. 2. Parity plots for methanol and carbon monoxide syntheses on the Ga_2O_3–Pd/silica catalyst using the 'competitive adsorption' model, variant 2379—see text (T = 538 K).

3.2. Steady-state, competitive hydrogen adsorption model

In a previous work, we were able to establish experimentally that the detrimental impact of high partial pressures of CO on the performance of the Ga_2O_3–Pd/silica catalysts is directly related to the strong chemisorption of carbon monoxide on the metal at reaction conditions, which then decreases the availability of atomic hydrogen on the gallia [12].

Within the framework of our former models, atomic hydrogen is made available to the reaction system via the reversible steps S10 (molecular hydrogen dissociation onto the Pd crystallites) and S11 (migration/transfer to the gallia phase), the first of which is known to be fast—or thermodynamically equilibrated. So, under steady-state conditions, the following stoichiometric (or mass-balance) constriction applies:

$$r_{11} = r_{H_2} = 3\, r_{CH_3OH} + r_{CO} \tag{18}$$

where

$$r_{11} = k_{11}[*][\text{H-}\bullet] - k_{-11}[\text{H-}*][\bullet] \tag{19}$$

The approach is entirely similar to those used by Chang-Yu and Froment [36] and Li and Delmon [37] while modeling hydrotreating processes. In our case, as CO competes with atomic hydrogen for surface Pd, the total amount of available metal sites is:

$$[\bullet]_{tot} = [\text{H-}\bullet] + [\bullet] + [\text{CO-}\bullet] \tag{20}$$

Using the conventional definition of surface coverage for CO:

$$\theta_{CO} = [\text{CO-}\bullet]/[\bullet]_{tot} \tag{21}$$

considering that under chemisorption equilibrium:

$$[\text{H-}\bullet] = \sqrt{K_{10}}\sqrt{p_{H_2}}[\bullet] \tag{22}$$

and operating on Eq. (20), the following expression results:

$$[\bullet] = \frac{[\bullet]_{tot}(1-\theta_{CO})}{1+\sqrt{K_{10}}\sqrt{p_{H_2}}} \tag{23}$$

where at any reaction temperature θ_{CO} can be calculated for each p_{CO}, employing experimental data taken with the Ga_2O_3–Pd/silica catalyst [12,15].

Defining the relationship $\alpha = [\text{H-}*]/[*]$, using Eqs. (22) and (23) and rearranging Eq. (19), a polynomial expression in α results:

$$\sqrt{K_{10}}K_{11}\sqrt{p_{H_2}} - \frac{r_{11}\left[1+\sum_{i=1}^{8} g_i(\alpha)\right]\left[1+\sqrt{K_{10}}\sqrt{p_{H_2}}\right]}{k_{-11}[\bullet]_{tot}[*]_{tot}(1-\theta_{CO})} - \alpha = 0 \tag{24}$$

where now each of the g_i terms (already presented in Table 3) is a function of α. Eq. (24) shows that whenever the supply of atomic hydrogen to the gallia surface is not rate-limiting, α reaches its maximum value, $\alpha_{eq} = \sqrt{K_{10}}K_{11}\sqrt{p_{H_2}}$. As above, a new kinetic rate constant $k'_{-11} = k_{-11}[\bullet]_{tot}[*]_{tot}$ can be defined to embed the physical features of the catalyst into a single parameter.

Next, after replacing the concentration of each reaction intermediate in terms of α, the expressions for r_3 and r_{12} presented in Eqs. (3)–(6) can be rewritten as follows:

$$r_3 = \frac{k''_3 p_{CO_2}\alpha^2(1-(p_{CH_3OH}p_{H_2O}/p^3_{H_2}p_{CO_2}K_{R1_1}(\alpha/\alpha_{eq})^6))}{D^2} \tag{25}$$

$$r_{12} = \frac{k''_{12} p_{CO_2}\alpha(1-(p_{CH_3OH}p_{H_2O}/p_{H_2}p_{CO_2}K_{R2}(\alpha/\alpha_{eq})^2))}{D} \tag{26}$$

in which

$$k''_3 = k_3K_1K_2[*]^2_T = \frac{k'_3}{K_{10}K^2_{11}} \tag{27}$$

$$k''_{12} = k_{12}K_1K_2[*]_T = \frac{k'_{12}}{\sqrt{K_{10}}K_{11}} \tag{28}$$

and, as above,

$$D = 1 + \sum_{i=1}^{8} g_i(\alpha)$$

Constants k'_3, k'_{12} and $\sqrt{K_{10}}K_{11}$ were already obtained using the 'competitive' adsorption model (excluding the subset of experiments with deliberate addition of CO). So, upon replacing the concentration of each reaction intermediate in terms of variable α, each newly calculated value of both responses, r_3 and r_{12}, can be used, inside a subroutine of the algorithm containing the polynomial equation in α, Eq. (24), to check whether the parameters found in the corresponding iteration give also a root of the polynomial (which they must). The strategy constitutes, therefore, a constrained optimization.

Within the context of the parameters format presented in Eq. (16) the new parameters needed to fully describe the dynamics of the reacting system under steady-state conditions, according to Eq. (24) are

$$k_{-11} = A_{-11}\exp\left(\frac{-\Delta E_{-11}}{RT}\right), \quad K_{10} = A_{10}\exp\left(\frac{-\Delta H_{10}}{RT}\right) \tag{29}$$

A calculated value of k_{11}, the direct kinetic rate constant given by Eq. (19), is of course also accessible through $K_{11} = k_{11}/k_{-11}$, once K_{10} is extracted from the convoluted parameter $\sqrt{K_{10}}K_{11}$, already obtained with the 'competitive' adsorption model.

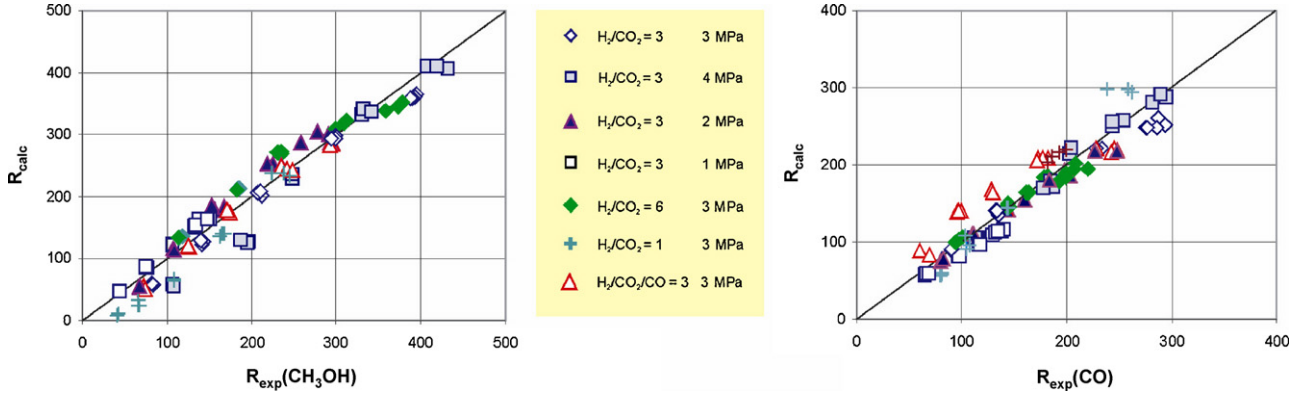

Fig. 3. Parity plots for methanol and carbon monoxide syntheses on the Ga_2O_3–Pd/silica catalyst using the steady state and the 'competitive adsorption' model, variant 2379—see text (T = 538 K).

Table 7
Additional parameter values for the steady-state, competitive adsorption model, variant 2379.[a].

Group source	Group component[b]	Value	Lower limit (95% conf. int.)	Upper limit (95% conf. int.)
K_{10}	A	3.33×10^{-25}	3.32×10^{-25}	3.34×10^{-25}
	$(-\Delta H)$	239.0	214.5	262.7
k_{-11}	A	$2.32 \times 10^{+11}$	$2.30 \times 10^{+11}$	$2.34 \times 10^{+11}$
	ΔE	63.02[#]	9.38	116.65

[a] These values were obtained by adding the sub-set of experimental points where CO was deliberately added to the reacting system. The relative residuals of each response within the subset were Res 1 = 8.3×10^{-3} and Res 2 = 7.14×10^{-2}, respectively (see Table 5).
[b] The values of the frequency factors shown in the table correspond to either Arrhenius or Van't Hoff propositions—see text. ΔE and ΔH values are given in kJ/mol.
[#] Non-significant.

Fig. 3 shows that the steady-state model succeeds in eliminating the bias from both parity plots. The calculated parameters were physicochemically consistent (i.e., they both had positive signs) only using the 2379 variant; however, k_{-11} was not significant at the required confidence level, probably because the number of data points taken using the ternary mixtures was insufficient. The relative residuals for each response were 8.3×10^{-3} and 7.14×10^{-2}, respectively (Table 7), which indicates that the goodness of fit was equivalent to that of the 'competitive' adsorption model.

4. Conclusions

The bifunctional synthesis pathway that leads to CH_3OH and CO on Ga_2O_3–Pd/silica catalysts using CO_2/H_2 mixtures operates through dissociation of molecular hydrogen on the palladium crystallites and further migration of atomic hydrogen to GaO_x, where a sequence of hydrogenation steps of the carbonaceous species operates. The reaction pathway can be adequately described, using the LHHW formalism.

Whenever the supply of atomic hydrogen to the gallia surface is sufficient, the most likely rate determining steps for the methanol synthesis and the RWGS reactions are the hydrogenation of formate to the fast reacting methylenebisoxy species, and the decomposition/dehydroxylation of formate to give CO(g), respectively.

A competitive adsorption mechanism, where adsorbed atomic hydrogen competes on the gallia for the same active sites occupied by the other surface intermediates, was found to be the most satisfactory, in terms of the physicochemical significance of the parameter estimates. Minimal residuals were found – for a wide range of process conditions – considering as kinetically relevant the simultaneous surface occupancy by formate, methylenebisoxy, hydroxyl and atomic hydrogen intermediates.

The deleterious 'interference' of CO for certain process conditions, such as high conversion and/or ternary $H_2/CO_2/CO$ mixture feeds, could be adequately modeled. In those cases CO, which chemisorbs strongly onto the Pd crystallites, competes with H_2, and severely limits the availability of atomic hydrogen (on)to the gallia phase. Using the steady-state approach, the supply and demand of atomic hydrogen were then balanced, to find the best model interpretation of the observed reactivity patterns. The steady-state model retained the mechanistic features of the 'competitive adsorption' model.

Acknowledgments

The financial support of CONICET, UNL and ANPCyT (PICT 14-25282) is gratefully acknowledged by the authors.

Appendix A. Supplementary data

Supplementary data associated with this article can be found, in the online version, at doi:10.1016/j.cej.2009.02.013.

References

[1] J.B. Hansen, in: G. Ertl, H. Knözinger, J. Weitkamp (Eds.), Handbook of Heterogeneous Catalysis, vol. 4, WILEY-VCH, 1997.
[2] C.V. Ovesen, B.S. Clausen, J. Schiøtz, P. Stoltze, H. Topsøe, J.K. Nørskov, Kinetic implications of dynamical changes in catalyst morphology during methanol synthesis over Cu/ZnO catalysts, J. Catal. 168 (1997) 133–142.
[3] P. Stoltze, Microkinetics simulation of catalytic reactions, Prog. Surf. Sci. 65 (2000) 65–150.
[4] R.M. Agny, C.G. Takoudis, Synthesis of methanol from carbon monoxide and hydrogen over a copper-zinc oxide-alumina catalyst, Ind. Eng. Chem. Prod. Res. Dev. 24 (1985) 50–55.
[5] G.H. Graff, E.J. Stamhuis, A.A.C.M. Beenackers, Kinetics of low pressure methanol synthesis, Chem. Eng. Sci. 43 (12) (1988) 3185–3195.
[6] K.M. Vanden Bussche, G.F. Froment, A steady-state kinetic model for methanol synthesis and the water gas shift reaction on a commercial $Cu/ZnO/Al_2O_3$ catalyst, J. Catal. 161 (1996) 1–10.
[7] A. Coteron, A.N. Hayhurst, Kinetics of the synthesis of methanol from $CO + H_2$ and $CO + H_2 + CO_2$ over copper-based amorphous catalysts, Chem. Eng. Sci. 49 (1994) 209–221.
[8] J. Weigel, R.A. Koeppel, A. Baiker, A. Wokaun, Surface species in CO and CO_2 hydrogenation over copper/zirconia: On methanol synthesis mechanism, Langmuir 12 (1996) 5319–5329.
[9] S.E. Collins, D.L. Chiavassa, A.L. Bonivardi, M.A. Baltanás, Hydrogen spillover in Ga_2O_3–Pd/SiO_2 catalysts for methanol synthesis from CO_2/H_2, Catal. Lett. 103 (2005) 83–88.
[10] S.E. Collins, M.A. Baltanás, A.L. Bonivardi, An infrared study of intermediates of methanol synthesis from carbon dioxide over Pd/β-Ga_2O_3, J. Catal. 226 (2004) 410–421.
[11] S.E. Collins, Characterization of Pd–Ga_2O_3 Based Catalysts Active to CO_2 Hydrogenation to Methanol by Infrared Spectroscopy, Doctoral Thesis, Universidad Nacional del Litoral, Argentina, 2005.
[12] D. Chiavassa, J. Barrandeguy, A.L. Bonivardi, M.A. Baltanás, Methanol synthesis from CO_2/H_2 using Ga_2O_3–Pd/silica catalysts: impact of reaction products, Catal. Today 133–135 (2008) 780–786.
[13] D.E. Mears, Tests for transport limitations in experimental catalytic reactors, Ind. Eng. Chem. Proc. Des. Dev. 10 (1971) 541–547.
[14] G.F. Froment, K.B. Bischoff, Chemical Reactor Analysis and Design, 2nd ed., Wiley, New York, 1990.
[15] J. Barrandeguy, Selective Hydrogenation of CO_2 Using Promoted Palladium Catalysts, Master Thesis, Universidad Nacional del Litoral, Argentina, 2002.
[16] A.L. Bonivardi, D.L. Chiavassa, C.A. Querini, M.A. Baltanás, Enhancement of the catalytic performance to methanol synthesis from CO_2/H_2 by gallium addition to palladium/silica catalysts, Stud. Surf. Sci. Catal. 130 (2000) 3747–3752.
[17] T. Fujitani, M. Saito, Y. Kanai, T. Watanabe, J. Nakamura, T. Uchijima, Development of an active Ga_2O_3 supported palladium catalyst for the synthesis of methanol from carbon dioxide and hydrogen, Appl. Catal. A: Gen. 125 (1995) L199–L202.
[18] T. Fujitani, I. Nakamura, Methanol synthesis from CO and CO_2 hydrogenations over supported palladium catalysts, Bull. Chem. Soc. Jpn. 75 (2002) 1393–1398.
[19] M.L. Poutsma, L.F. Elek, P.A. Ibarbia, A.P. Risch, J.A. Rabo, Selective formation of methanol from synthesis gas over palladium catalysts, J. Catal. 52 (1978) 157–168.
[20] A. Erdöhelyi, M. Pásztor, F. Solymosi, Catalytic hydrogenation of CO_2 over supported palladium, J. Catal. 98 (1986) 166–177.
[21] I.A. Fisher, A.T. Bell, In-situ infrared study of methanol synthesis from H_2/CO_2 over Cu/SiO_2 and $Cu/ZrO_2/SiO_2$, J. Catal. 172 (1997) 222–237.
[22] I.A. Fisher, A.T. Bell, In-situ infrared study of methanol synthesis from H_2/CO over Cu/SiO_2 and $Cu/ZrO_2/SiO_2$, J. Catal. 178 (1998) 153–173.
[23] I.A. Fisher, A.T. Bell, A mechanistic study of methanol decomposition over Cu/SiO_2, ZrO_2/SiO_2, and $Cu/ZrO_2/SiO_2$, J. Catal. 184 (1999) 357–376.
[24] S.E. Collins, M.A. Baltanás, J.L. García Fierro, A.L. Bonivardi, Gallium–hydrogen bond formation of gallium and gallium–Pd silica supported catalyst, J. Catal. 11 (2002) 252–264.
[25] S.E. Collins, M.A. Baltanás, A.L. Bonivardi, Infrared spectroscopic study of the carbon dioxide adsorption on the surface of Ga_2O_3 polymorphs, J. Phys. Chem. B 110 (2006) 5498–5507.

[26] S.E. Collins, M.A. Baltanás, A.L. Bonivardi, Heats of adsorption and activation energies of surface processes measured by infrared spectroscopy, J. Mol. Catal. A: Chem. 281 (2008) 73–78.
[27] M. Haneda, E. Joubert, J.C. Ménézo, D. Duprez, J. Barbier, N. Bion, M. Daturi, J. Saussey, J.C. Lavalley, H. Hamada, Surface characterization of alumina-supported catalysts prepared by sol–gel method. Part II. Surface reactivity with CO, Phys. Chem. Chem. Phys. 3 (2001) 1371–1375.
[28] S.E. Collins, L.E. Briand, L.A. Gambaro, M.A. Baltanás, A.L. Bonivardi, Adsorption and decomposition of methanol on gallium oxide polymorphs, J. Phys. Chem. C 112 (2008) 14988–15000.
[29] D. Martin, D. Duprez, Mobility of surface species on oxides. 2. Isotopic exchange of D_2 with H of SiO_2, Al_2O_3, ZrO_2, MgO, and CeO_2: activation by rhodium and effect of chlorine, J. Phys. Chem. B 101 (1997) 4428–4436.
[30] R.C. Reid, J.M. Prausnitz, T.K. Sherwood, B.E. Poling, The Properties of Gases and Liquids, 4th ed., McGraw-Hill, New York, 1987.
[31] R.G. Herman, K. Klier, G.W. Simmons, B.P. Finn, J.B. Bulko, T.P. Kobylinski, J. Catal. 56 (1979) 407–429.
[32] Y. Bard, Nonlinear Parameter Estimation, Academic Press Inc., New York, 1974.
[33] W.E. Stewart, M. Caracotsios, J.P. Sørensen, Parameter estimation from multiresponse data, AIChE J. 38 (1992) 641–650.
[34] T. Chang, R.W. Rousseau, P.K. Kilpatrick, Methanol synthesis reaction: calculation of equilibrium conversions using equations of state, Ind. Eng. Chem. Proc. Des. Dev. 25 (1986) 477–481.
[35] G.H. Graaf, P.J.J.M. Sijtsema, E.J. Stamhuis, G.E.H. Joosten, Chemical equilibria in methanol synthesis, Chem. Eng. Sci. 41 (1986) 2883–2890.
[36] Y. Chang-Yu, G.F. Froment, Rate equations for the modeling of the synergy in multicomponent catalysts with interconversion of active sites, Chem. Eng. Sci. 46 (1991) 3177–3188.
[37] Y.W. Li, B. Delmon, Modelling of hydrotreating catalysis based on the remote control: HYD and HDS, J. Mol. Catal. A: Chem. 127 (1997) 163–190.